THE DISPATCH

Volume 4, Issue 1 | Defense Threat Reduction Information Analysis Center | April 2014

This Issue

Contact Us

dtriac@dtra.mil
or visit us at
www.dtriac.dtra.mil

From the Program Manager

Welcome to the second issue of *The Dispatch* for the year 2014. This is the second of two issues that features articles from the Nuclear Technologies personnel, describing studies and efforts related to high-altitude nuclear effects (HANE) phenomenology. Last quarter, we introduced you to HANE phenomenology. This quarter, we will delve into research related to DTRA's HANE phenomenology partnerships, including the Large Plasma Device (LAPD) at UCLA.

On a somber note, our community recently lost a respected colleague. Mr. John G. Lewis died peacefully Sunday, 23 February 2014, in Roseville, California, at the age of 88 years. Mr. Lewis was involved in nuclear weapons effects testing and research for nearly 60 years. In addition to his many, many contributions, he was considered the founder of Project Graybeard. Because of his efforts, the first-hand knowledge attained by the scientists who actively participated in nuclear testing has been preserved for future analysis.

Please contact us directly if you ever have any questions or comments related to DTRIAC at dtriac@dtra.mil.

Thanks,

Joyce Rowell
DTRIAC Program Manager

John G. Lewis (1925–2014)

Mr. John G. Lewis began his career defending our nation by serving in the Navy from 1944 to 1946. After obtaining a Master's of Science Degree in Nuclear Physics, he went to work for the U. S. Army Corps of Engineers. While at the Army Corps of Engineers, he was an experimenter on 13 atmospheric nuclear tests. Joining the Armed Forces Special Weapons Project (AFSWP) (later DASA, DNA, and DTRA), Mr. Lewis was involved in 7 atmospheric events and 11 underground events. Culminating his government career in 1974, Mr. Lewis went on to work for R&D Associates until he retired in 1990. Even after retirement, Mr. Lewis continued to support the nuclear community as a consultant. In 1993, he became the inaugural Project Graybeard leader for Shock Physics and Domain Coordinator for Nuclear Sources. He was also a charter member of the Data Archival and Retrieval Enhancement (DARE) Data Review Group, creating a synergy between Graybeards and the DARE Program. Mr. Lewis's numerous contributions were recognized through multiple awards, including the Defense Nuclear Agency Exceptional and Meritorious Service award, the Department of Defense Meritorious Service award, and the Defense Threat Reduction Agency Lifetime Achievement Award.

Understanding the Structure of an Artificial Electron Radiation Belt from a HANE

by M. M. Cowee (LANL)

Beta-decay of fission fragments after a high-altitude nuclear explosion (HANE) produces energetic electrons (MeV energies) which can become trapped in the earth's geomagnetic field, forming an artificial radiation belt that poses a threat to satellites. Several legacy models have been developed, for example the Satellite Nuclear Threat Assessment Code System (SNRTACS), to predict the properties of an artificial belt based on our current physical understanding of the processes involved and the limited data available from space- and ground-based observations after the HANE test shots in 1962. Unfortunately, the observations did not necessarily show a clear picture of the phenomena, possibly due to insufficient spatial and temporal coverage and insufficient measurements at fission-spectrum energies, or unexpected physical behavior. For example, the observations suggest that beta-decay electrons were detected at radial distances beyond that of the burst region (Walt, 1966), an effect which has yet to be explained in the approximately 50 years since the STARFISH PRIME test.

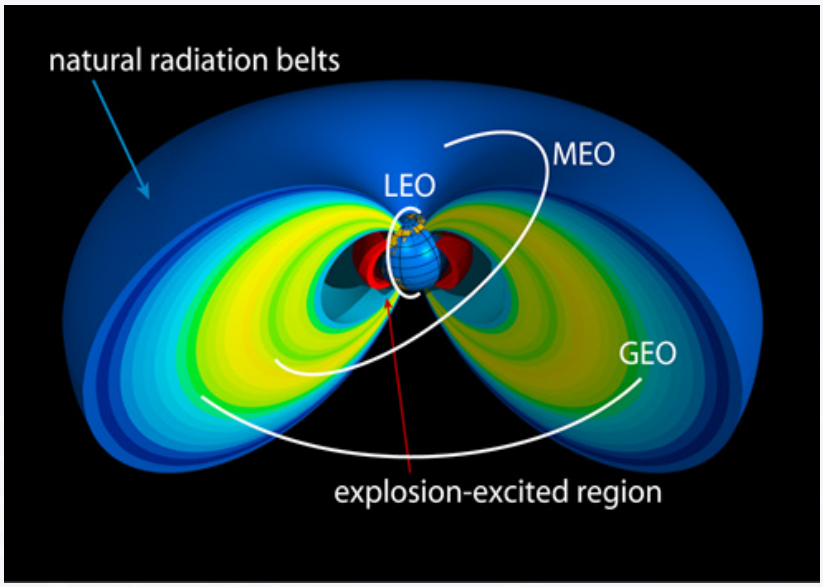

Schematic of the Earth's radiation belts and example orbits for spacecraft in low-, medium-, and geostationary-Earth orbit (LEO, MEO, and GEO). A hypothetical artificial radiation belt in the LEO region is indicated in red. Courtesy Michael Henderson.

To better understand the properties of an artificial belt from a basic physics perspective, DTRA is supporting efforts at LANL to model the formation of the belt in the first seconds after the burst and its subsequent decay over months to years after the burst. On short timescales (e.g., seconds to minutes after the burst), we use the analytic Electron Source Model (ESM) developed at LANL (Cowee, et al., 2012), which predicts the initial spatial and velocity distribution of the debris ions and beta-decay electrons as a function of the burst yield and location. The ESM calculations for the size of the burst region and the initial velocity distribution of the debris ions are currently guided by results from hybrid (kinetic ion, fluid electron) computer simulations of the expanding debris ion cloud (Winske and Gary, 2007). We hope to better constrain the input parameters based on the results of laser-target experiments being conducted at UCLA.

The ESM predicts that the trapped beta-decay electrons will have a highly anisotropic velocity–space distribution, which could be unstable to plasma waves. Such types of plasma waves could scatter the electrons into the atmosphere on timescales of a fraction of a second. To investigate this effect, we carry out particle-in-cell (PIC) computer simulations of the growth of both electrostatic and electromagnetic plasma waves driven by the beta-decay electrons. Our initial results suggest these waves are indeed important and may cause the rapid precipitation of artificial belt electrons on short timescales after the burst; such effects are not currently included in any artificial belt models but would be a critically important addition.

To model the decay of the artificial belt on longer timescales we use the Dynamic Radiation Environment Assimilation Model (DREAM) diffusion code developed at LANL (Reeves, et al., 2012). DREAM is used primarily for natural radiation belt studies, but the ESM results can be input to DREAM to provide an artificial belt source term. DREAM then evolves the artificial belt due to the natural radiation belt processes: solar wind compression of the magnetosphere causes low-frequency waves that radially diffuse the electrons, plasma flows and lightning can generate high-frequency waves that cause diffusion in velocity space and energy, and Coulombic interactions between the trapped electrons and the atmosphere also cause diffusion in velocity-space and energy.

Understanding the Structure of an Artificial Electron Radiation Belt from a HANE *(continued)*

Diffusion coefficients are based on different empirical and theoretical models (Brautigam and Albert, 2000; Summers, 2005) and are dependent on the geomagnetic storm level. With this technique, we can model the spatial and energy structure of the artificial belt at days to years after the burst and investigate how long it could take for an artificial belt to decay away.

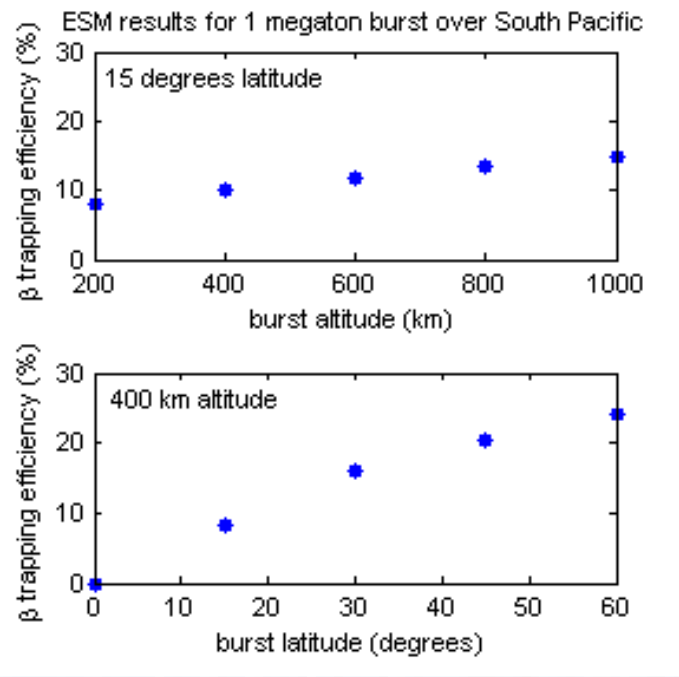

ESM results for the trapping efficiency of the beta-decay electrons for a 1-MT burst over Johnston Island in the South Pacific (top) for varying altitude at 15° latitude, and (bottom) varying latitude at 400 km altitude.

REFERENCES

Brautigam, D. and J. Albert (2000), "Radial diffusion analysis of outer radiation belt electrons during the October 9, 1990, magnetic storm," *Journal of Geophysical Research,* 105.

Cowee, M. M., G. S. Cunningham, D. Winske, and G. D. Reeves (2012), "Initial comparison of the Los Alamos HANE energetic electron source model with HANE test data," 2012 HEART Conference, Monterey, CA.

Reeves. G. D., Y. Chen, G. S. Cunningham, R. W. H. Friedel, M. G. Henderson, V. K. Jordanova, J. Koller, S. K. Morley, M. R. Thomsen, and S. Zaharia (2012), "Dynamic Radiation Environment Assimilation Model: DREAM," *Space Weather,* 10, S03006.

Summers D. (2005), "Quasi-linear diffusion coefficients for field-aligned electromagnetic waves with applications to the magnetosphere," *Journal of Geophysical Research,* 110.

Walt, M. (1966), "Overall analysis of experiments on artificial radiation belts," *Radiation Trapped in the Earth's Magnetic Field,* B. M. McCormac, ed., D. Reidel Publishing Co., Holland, 666-670.

Winske, D. and S. P. Gary (2007), "Hybrid simulations of debris-ambient ion interactions in astrophysical explosions," *Journal of Geophysical Research,* 112.

Understanding Debris-Background Ion Interactions in High-Altitude Nuclear Explosions

by D. Winske (LANL)

The STARFISH PRIME event produced many interesting nuclear, electromagnetic, atomic, and plasma effects, which have led over the past 50 years to much research in understanding the overall phenomenology of high-altitude nuclear explosions (HANE). At altitudes lower than STARFISH, where collisional processes come into play, the physics of a nuclear fireball in the atmosphere is well understood. But at high altitudes, where collisions are much weaker, the fundamental issue of how the ionized weapon debris is stopped in the ionosphere in order to produce a relatively localized debris cloud remains unresolved. In the last 30 years, this issue has been investigated in the laboratory using high-power lasers to simulation the explosion and subsequent expansion of the debris plasma. While experiments that were carried out on the Helios laser at Los Alamos and then later on the Pharos laser at the Naval Research Laboratory (NRL) were able to produce some plasma conditions representative of the HANE environment and obtained interesting results, they were not very successful in addressing the basic debris-air coupling problem in the collisionless regime. This problem is being revisited in a new DTRA-funded experimental program with the 500-J Raptor glass laser on the Large Plasma Device (LAPD) at the University of California, Los Angeles (UCLA).

It is well known that in high-altitude explosions, the debris ions initially stream from the burst point at super-Alfvenic speeds, are slowed down, and eventually stopped. The debris acts like a magnetic piston to produce an outgoing magnetosonic shock wave that carries momentum and energy away from the burst region. This

Understanding Debris-Background Ion Interactions in High-Altitude Nuclear Explosions *(continued)*

process is shown schematically in Figure 1. Using both experiments and numerical simulations, we are addressing the following issues: What is the mechanism by which the debris ions are stopped? Under what conditions can a shock wave be generated? How do the properties of the shock scale with the plasma parameters? Can we easily measure properties of the shock and debris to verify and validate the underlying physical processes? The initial experiments conducted by the UCLA group on the LAPD facility have been very encouraging. In addition to the new experimental capability, optimism that this issue can finally be put to rest also derives from two theoretical advances. First, there has been continued progress in the development of improved numerical simulation models, in which the ions are treated as particles and the electrons as a massless fluid, running on massively parallel computers. These codes have demonstrated the importance of magnetic field effects, rather than electric fields due to charge-separation, pressure gradients, or plasma waves, in stopping the debris ions. Second, the results of 3-D simulations of HANE-like debris expansion, supplemented by simpler 1-D calculations, have led to a new understanding on how the debris ions are stopped while the background ions are accelerated radially as an outward propagating shock is formed. Simulation studies for the UCLA experimental conditions have shown that magnetic shock waves will be readily generated in this facility when the background plasma density is increased by an order of magnitude later this year. The improved conditions will allow the new theoretical insights to be experimentally verified and shed significant light on the nature of the coupling between the debris and background ions.

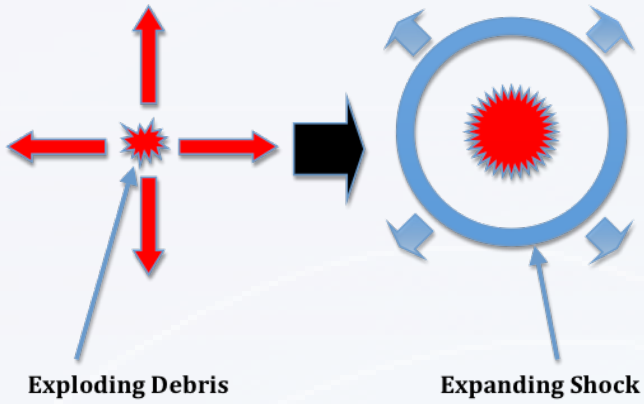

Figure 1. Expanding debris ions from a nuclear (or laser) explosion (left) are stopped by the background plasma and magnetic field, giving rise to a shock wave propagating out from the burst region into the ambient plasma (right).

To model the experiment, we consider a 2-D planar (x, y) configuration with the ambient magnetic field (**B** = B_o**z**) perpendicular to the simulation plane. We assume the debris ions are emitted from a small slab-like region near the left end (in x) of the simulation box centered in y. We do not model the laser-target interaction, but merely allow all the debris ions to expand outward from this region radially, with a directed velocity mostly directed along x, but with some angular spread. Here we assume that the debris ions are carbon C^{+4}, hydrogen is the background ion species with density $2 \cdot 10^{13}$ cm^{-3} and the ambient magnetic field B = 300 G, corresponding to the characteristic speed in a magnetized plasma of an Alfven wave, v_A = 144 km/s. The debris streaming velocity is V_d = 300 km/s, corresponding to an initial Alfven Mach number of the debris ions V_d/v_A = 2.1. The system size of the simulation is 100 by 100 cm, comparable to that in LAPD. Figure 2 presents the results of a simulation at t = 2 μs, showing a 2-D color contour plot of the magnitude of

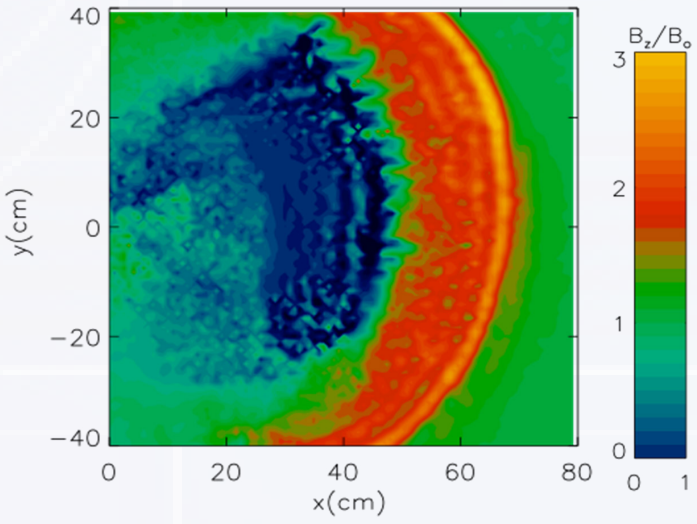

Figure 2. Results of simulation of expansion of C^{+4} debris ions into a hydrogen plasma showing contours of the magnetic field magnitude B_z/B_o at t = 2 μs, showing magnetic cavity (blue region) and shock wave (yellow-red) propagating to the right.

Understanding Debris-Background Ion Interactions in High-Altitude Nuclear Explosions *(continued)*

the magnetic field. The plot indicates that the wedge-shaped debris plasma has created a magnetic cavity (blue). The debris ions have come to rest at the outer edge of the cavity. Prominent striations appear at the front of the cavity where there are strong magnetic field and density gradients. To the right of the cavity is an outward propagating shock (red), with a well-defined, steepened leading front edge (yellow). The Alfven Mach number of the shock is $V_{shock}/v_A = 2.4$, characteristic of shock waves in the collisionless HANE regime. Detailed analysis of the simulations confirms the validity of the basic mechanism of how the debris ions are stopped and the shock wave is generated and suggests diagnostics that can confirm this process in the experiments.

Eventually, studies like these will lead to a more comprehensive understanding of debris dynamics in high-altitude nuclear effects, where a number of different ion masses and charge states exist in both the debris and the background plasmas.

Collaborators: M. M. Cowee (LANL), S. E. Clark and C. Niemann (UCLA), and D. J. Larson and S. H. Brecht (LLNL). References to material in the text can be found in: D. Winske, M. M. Cowee, C. Niemann, D. J. Larson, and S. H. Brecht, "Debris background ion interaction and collisionless shock formation in a helium plasma," *Journal of Radiation Effects,* Vol. 31, submitted 2013.

Controlled Space Physics Experiments Using Laboratory Magnetospheres

by M. E. Mauel, D. Garnier, J. Kesner, T. Roberts, M. Worstell, and A. Cole (Columbia University and MIT)

During the past decade, we have built and operated two laboratory magnetospheres and discovered techniques to observe, understand, and control the dynamics of plasma and artificial radiation belts confined by a dipole magnetic field. Laboratory magnetospheres permit controlled testing of space weather models in relevant magnetic geometry by observing dynamics following the injection of heat, particles, and electromagnetic perturbations. In laboratory magnetospheres, plasmas exhibit complex interchange instability (Phys. Rev. Lett, 2003; Phys Plasmas, 2006), strong convection (Phys. Rev. Lett., 2005), self-organization (Nature Phys. 2010), and sustained turbulent mixing (Phys. Rev. Lett., 2010). The simplicity of the dipole magnetic field permits "whole-plasma" imaging, detailed tests of space-weather models, and the potential to develop new insights about energetic particle events that may occur in the Earth's magnetosphere.

To illustrate the capabilities of laboratory magnetospheres, we've conducted new experiments designed to observe the dynamics following small mass "explosions" triggered by the injection of pellets, containing hydrogen and carbon, into an artificial radiation belt of highly energetic electrons. The large amount of hot material that forms when the pellet ionizes fills a magnetic flux tube and significantly disturbs the space environment and the radiation belts. Our experiments revealed the fast dynamics following the mass injection using simultaneous measurements of auroral currents, magnetic disturbances, and high-speed visible light videography. Our goals are to use these observations to advance modern modeling techniques and to test predictive models for space effects following a rapid mass/energy event.

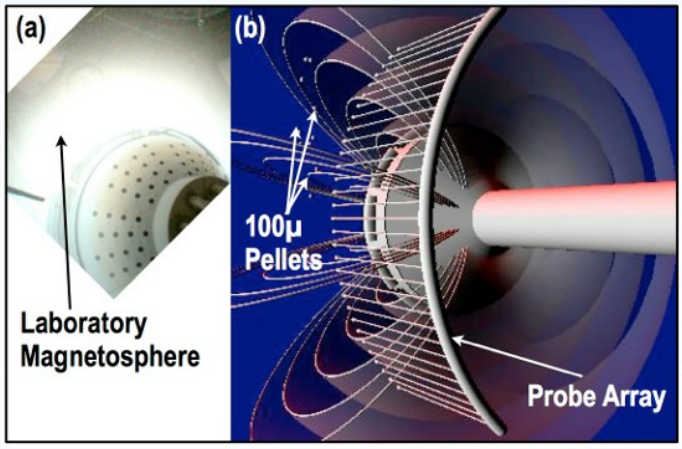

Figure 1. Laboratory magnetosphere at Columbia University showing (a) the bright light from the dense plasma near the strong dipole magnet and (b) the geometric arrangement of the pellet injection experiments.

Figure 1 illustrates the "exploding" pellet injection experiments at the smaller laboratory magnetosphere located at Columbia University. A laboratory magnetosphere is created with microwave heating, and the artifi-

Controlled Space Physics Experiments Using Laboratory Magnetospheres *(continued)*

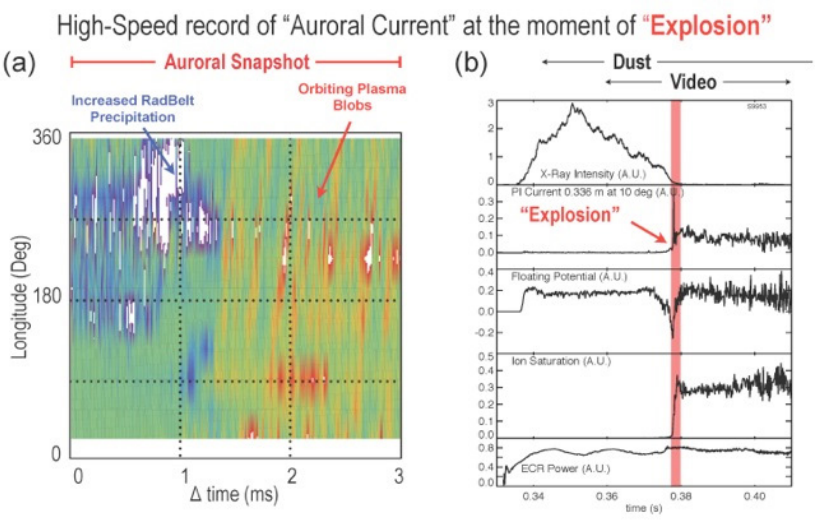

Figure 2. (a) High-speed record of the auroral current at the moment of explosion of a 100-μm polystyrene pellet shows increased precipitation of the artificial radiation belt followed by dense plasma-filled flux tubes that orbit every 200 μs. (b) A longer time record of decay of the artificial radiation belt due to the dust injection and showing the instant when the pellet exploded.

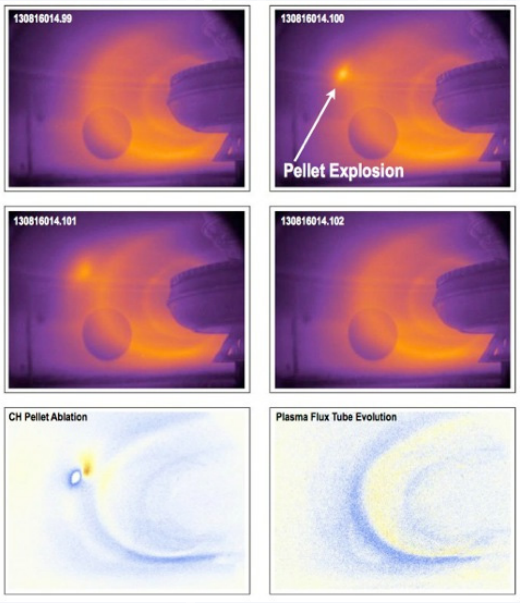

Figure 3. Records of an exploding 100-μm pellet in the world's largest laboratory magnetosphere at MIT. The top four frames span 66 ms, showing how quickly pellets evaporate when they reach hot plasma. The bottom two frames were made by taking the difference between video images (blue represents increasing light and yellow decreasing light.) They show (bottom left) the change of the visible light emission and (bottom right) the rate of inward injection of carbon, which is later swept out as the plasma returns to its usual quasi-steady state.

cial radiation belt is monitored by x-ray emission. Dozens of 100-μm polystyrene dust particles are dropped vertically into the plasma. When the dust pellets explode (as shown in Figure 2), the released plasma and neutral particles cause rapid precipitation of energetic electrons and the creation of plasma-filled magnetic flux tubes that orbit around the magnetosphere. Figure 2 shows a time-record of the auroral currents as measured by an array of polar current detectors that measure the energetic radiation belt loss current (shown in blue) and the loss current of magnetospheric ions (shown in red.)

The world's largest laboratory magnetosphere, located at MIT, creates magnetospheres with much higher density due to its larger size, higher power, and strong superconducting dipole magnet (Phys. Plasmas, 2006; Nature Phys., 2010). When pellet injection experiments were conducted in the larger experiment, we found the 100 μm dust pellets unable to penetrate deep into the regions having the most intense radiation belt particles. Nevertheless, the pellet injection caused significant modifications of the magnetospheric profiles and drove interchange mixing of plasma flux tubes that were clearly visible with whole-plasma videography.

Figure 3 shows the visible light images of one of many examples of exploding pellets that have been recorded in the large laboratory magnetosphere at MIT. When the frame-by-frame difference image is computed, the change of the visible light emission shows the inward injection of particles, which are swept out as the plasma returns to its usual quasi-steady state. These observations have motivated follow-on experiments when even larger pellets will be injected into the intense artificial radiation belt at higher speeds. The goals of these experiments are to create more energetic magnetospheric perturbations, explore impulsive methods to increase plasma density, and provide measured input with which to compare to space-weather simulations.

These experiments are part of our long-range research plan to explore higher density laboratory magnetospheres created with pellet injection and with higher power plasma heating. As the plasma density increases, the ion inertial length, c/ωpi, decreases. Important new experiments will become possible like Alfvén wave spectroscopy in relevant magnetic geometry and the observation of Alfvén pulsations excited by external

Controlled Space Physics Experiments Using Laboratory Magnetospheres *(continued)*

magnetic perturbations. Additionally, the production of higher plasma density in laboratory magnetospheres allow electromagnetic whistler waves to penetrate and refract at high magnetic field (Nature, 2010) and will make possible tests of chorus refraction, hiss generation, and wave-induced precipitation of trapped radiation belt particles.

References

Phys. Rev. Lett., 90, 185001 (2003).
Phys. Plasmas, 13, 056111 (2006).
Phys. Rev. Lett., 105, 205004 (2010).
Phys. Rev. Lett., 94, 175002 (2005).
Nature Phys., 6, 207 (2010).
Nature, 467, 943 (2010).

Scaled HANE Experiments with Laser-Produced Exploding Plasmas in the LAPD

by C. Niemann (UCLA), D. Winske (LANL), and D. Larson (LLNL)

Laboratory experiments with rapidly exploding laser-produced plasmas can be designed to investigate the coupling of energy and momentum between a super-Alfenic expanding debris cloud and a magnetized, ambient plasma in the context of high-altitude nuclear explosions (HANE). Scaled laboratory experiments can potentially provide new insight into the physics of HANES, including the formation of a shock and the transport of debris ions across the shock ramp. For example, data recorded during the STARFISH PRIME event has revealed debris ions at altitudes many times higher than the blast-radius, an observation that is still not fully understood (Dyal, 2006).

Laboratory shock experiments are unique in that the ratio between the size of the exploding debris cloud and the debris ion Larmor radius is of order unity and thus quite similar to that in HANES but significantly smaller than in space and astrophysical explosions. Details of the coupling physics will thus critically affect shock formation, providing a test-bed where the physics of debris-ambient coupling can be studied in great detail.

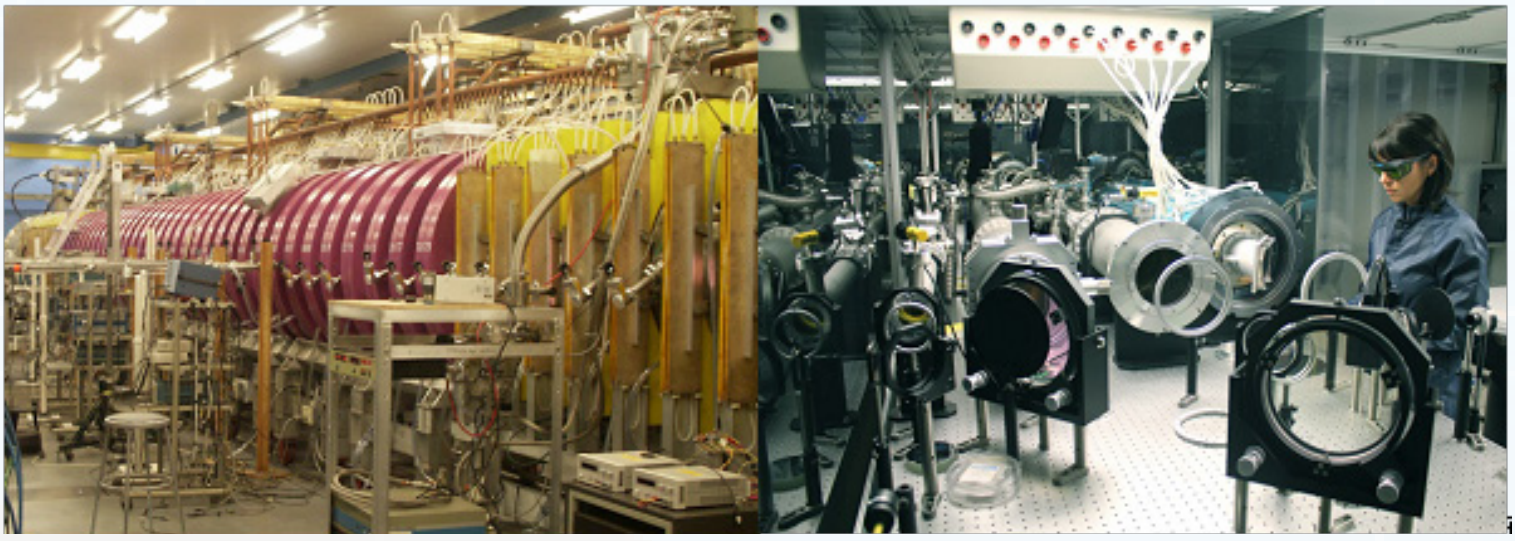

Figure 1. The Large Plasma Device and the Raptor kilojoule-class laser facility at the University of California, Los Angeles

Scaled HANE Experiments with Laser-Produced Exploding Plasmas in the LAPD *(continued)*

A new class of laser experiments has recently been funded by DTRA to study debris-ambient coupling in the laboratory. The experiments employ the Raptor kilojoule-class laser and the Large Plasma Device (LAPD) at the University of California, Los Angeles, uniquely combining an energetic super-Alfvenic debris could with a large (17 m by 0.5 m), highly magnetized, current-free, quiescent, well-characterized, and highly accessible ambient plasma (Niemann, et al., 2012).

In the experiment, a rapidly exploding plasma-cloud is produced by irradiating a solid target embedded in the preformed magnetoplasma with a high-power laser pulse. Focusing the beam to a 0.5-mm spot on a graphite target at an average intensity around 10^{13} W/cm^2 ablates more than 10^{17} debris ions at a bulk velocity of 500 km/s. The plasma plume blows off perpendicularly to the target surface and the external magnetic field. Prior to the laser pulse, the ambient plasma is created by an electric discharge between a cathode and an anode grid on one side of the machine and is maintained for several milliseconds. The plasma column is formed by impact ionization of a gas-fill in a steady, axial magnetic field of several hundred Gauss, and the plasma is current free. On the hydrodynamic time scales of the laser-plasma, the ambient-plasma is essentially stationary.

A laser-driven magnetic piston is used to transfer momentum to the stationary ambient plasma. Initially, the laser-plasma energy density exceeds the magnetic field energy density, and the dynamics of the exploding laser-plasma is only marginally affected by the background magnetic field. However, the plasma's finite conductivity and frozen-in magnetic flux lead to an expulsion and distortion of the magnetic field lines and the creation of a diamagnetic cavity. Azimuthal electric fields at the bubble edge, due to the relative motion of debris and ambient ions, decelerate the debris ions and accelerate the ambient ions via Larmor-coupling.

Figure 2 shows magnetic probe measurements of the formation and collapse of the diamagnetic cavity that is formed by a laser-produced carbon-plume exploding into He^+ plasma at super-Alfvenic speed ($M_A = 1.5$). The laser energy in these experiments was only 20 J. A magnetic cavity of 20 cm in diameter is formed (black area). We observe a field compression of 50% and a magneto-sonic pulse that separates from the cavity at later times (Niemann, et al., 2013). The bubble collapses after 1 μs and several orders of magnitude faster than predicted by classical field diffusion, indicative of the growth of plasma fluctuations in the current layer.

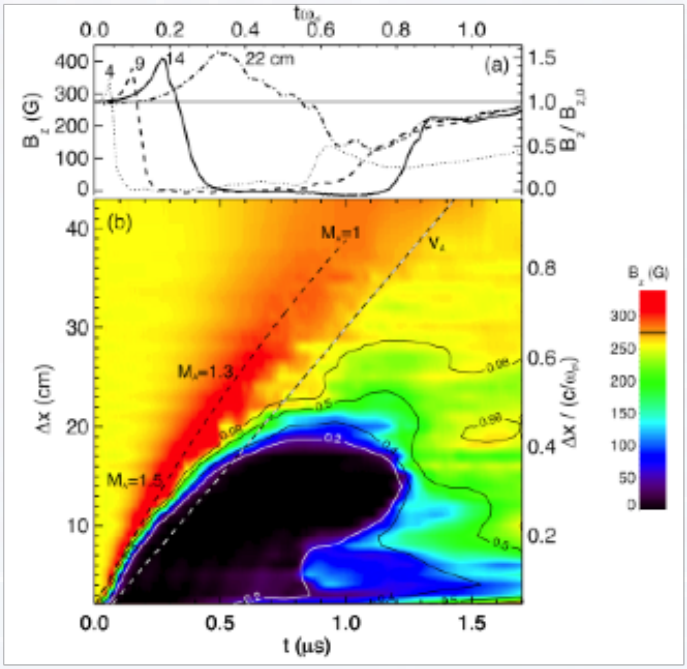

Figure 2. Magnetic-flux probe measurements of the evolution and collapse of a diamagnetic bubble in the LAPD. A magnetic pulse propagates out at $M_A = 1.5$, slowing as it separates from the bubble. The field compression is consistent with the Rankine-Hugoniot jump conditions.

Plasma densities in these initial experiments were limited to $2 \cdot 10^{12}$ cm^{-3} by the emissivity of the cathode. As a consequence, the Alfenic Much number was limited to $M_A = 1.5$, the bubble was too small (in relevant scale length), and a full-blown shock could not separate from the bubble. The measured field compression was consistent with the jump conditions for a shock.

A new plasma source has recently been installed that supports densities in excess of 10^{13} cm^{-3} and experiments with higher Mach-numbers ($M_A > 3$) and bubbles of several ion-inertial length (or Larmor radii) in size. Two-dimensional hybrid simulations performed for these ambient plasma parameters and laser energies of 500 J predicts the formation of a magnetosonic shock wave with relevance to HANES (Clark, et al., 2013). The streak plots in Figure 3 show the simulation over time versus position across the magnetic field. The magnetic

Scaled HANE Experiments with Laser-Produced Exploding Plasmas in the LAPD *(continued)*

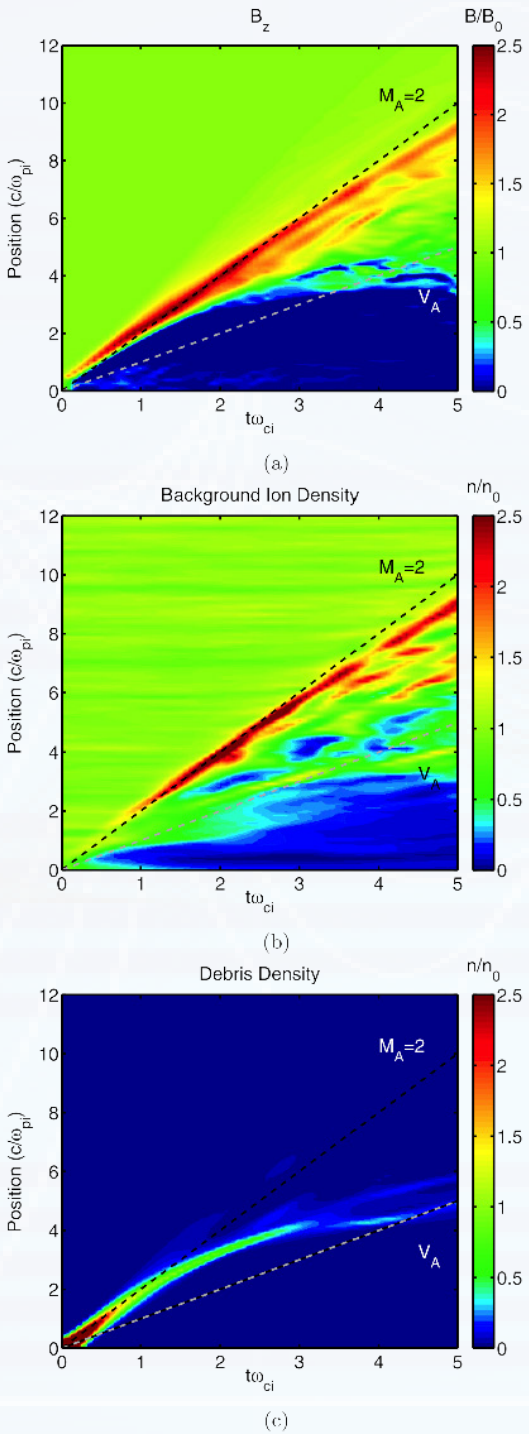

Figure 3. 2-D hybrid simulations of a magnetosonic shock (M_A=2) in the LAPD, showing the evolution of (a) the magnetic field, (b) the ambient density, (c) and the debris density.

field profile in Figure 3a shows a diamagnetic bubble that is roughly the size of the equal mass radius. It also shows a double compression feature that is present after the shock wave separates from the piston and propagates out. In this simulation, the initial blow-off speed is $M_A \sim 2$, which is the initial bubble formation velocity. At $t\omega_{ci} \sim 1$, the magnetic pulse slows as the debris slows. Later, the magnetic pulse speeds up as it separates from the bubble and propagates outward. Figure 3b shows that coupling occurs since the ambient ions are depleted from the central region of the bubble. Outside the bubble, the magnetic pulse is carried by the ambient ions. During the time that the pulse speeds up ($t\omega_{ci} \sim$ 1-3), it also steepens into a $M_A \sim 2$ shock. The density and magnetic field compressions of this shock are consistent with the Rankine-Hugoniot jump conditions. Figure 3c shows the debris ions slowing down, mostly concentrated in a shell. The bulk of the debris ions stop at the bubble edge, but there are a number of fast ions that are out in front of the compression. The phase space (not shown) shows a population of reflected background ions at the foot of the magnetic pulse, which provides the dissipation mechanism for the shock.

In future experiments, transport of both the debris and the ambient ions across the shock ramp will be studied in great detail using spectroscopy and laser fluorescence. Coupling will be compared for various ambient plasma and debris-cloud parameters to benchmark simulations codes.

References

Dyal, P. *J. Geophys. Res.* 111, A12211 (2006)

Clark, S.E., et al., *Phys. Plasmas* 20, 082129 (2013)

Niemann, C. et al., *J. Instrum.* 7, P03010 (2012)

Niemann, C. et al., *Phys. Plasmas* 20, 012108 (2013)

Schaeffer, D.B., et al., *Phys. Plasmas* 19, 070702 (2012)

In Memory of

by Gene Sevin

I first met John Lewis in the late 1950s when he was with the Armed Forces Special Weapons Project (AFSWP). John designed and managed intra-service R&D programs to advance the science of nuclear weapons effects (NWE) and the engineering of advanced protective structures. A new era of physics and civil engineering was beginning, and John was instrumental in empowering the Armed Services to develop NWE capabilities through their participation in nuclear weapons tests. In 1974, John left DNA (the result of several reorganizations since AFSWP) and government service to join the senior staff of RDA, where he remained until his retirement, still a trusted advisor to DNA.

John was a great inspiration to many. Although mild-mannered and always the perfect gentleman, he was tenacious in his beliefs and influential in bringing the best and brightest researchers into the field of NWE. He also had a strong influence on cooperation in NWE technologies and protective construction among our NATO allies.

Over the years, John made numerous contributions to the science of NWE, nuclear testing, protective structures design, the preservation of knowledge in these areas, and collectively to the national security. Let me cite three examples of John's outstanding contributions.

The moratorium against nuclear testing in the atmosphere moved nuclear testing underground. From the perspective of DOD, whose interest was NWE on equipment and operational components (particularly x-ray exposure), underground tests posed serious test execution problems, particularly in providing safe posttest access to the test chambers without allowing radiation leakage to the atmosphere. John led a successful effort to develop a test design that allowed for early-time radiation exposure within the mountain before completely shutting down the test chambers to allow later access to the experiments. In the public arena, an invention of that magnitude certainly would have gotten an award or two.

John was very concerned about making the vast body of technical information from the U.S. nuclear tests readily accessible to DOD researchers and military planners. He was acutely aware of potential loss in historical knowledge as the original experimenters passed from the scene. As a result, John conceived the Graybeard Project as a means of providing roadmaps through the experimental database. At his instigation, DTRA implemented the Graybeard Project, a multiyear (1991–1998) effort that later became known as the Nuclear Weapons Effects Technology Information (NWETI) project. Thirty-two guides were produced covering nuclear sources, shock physics, effects on structures, ionizing and electromagnetic radiation, thermomechanical effects, and biological effects. These guides were prepared in most instances by individuals who had participated in the original nuclear tests. John authored the Nuclear Sources guide and contributed to the Shock Physics guide. The NWETI project was a mammoth undertaking and will long redound to John's credit.

DNA was actively engaged with the Air Force when the MX missile program was developing a survivable basing system. Approximately 32 candidate basing schemes were in play. A promising basing candidate was the superhard silo, but it was feared that it could not survive the cratering effects of a near-miss weapon, especially as the trend in increasing missile delivery accuracy seemed clear. The size of a crater caused by an impacting nuclear weapon was something of a technology mystery in that theoretical predictions were considerably smaller in size than the craters measured at the Pacific Proving Grounds (PPG). This discrepancy generally was believed to be a shortcoming of theoretical models. But John thought it likely that final crater size at PPG was caused by late-time collapse of the atoll's coral structure, so that what was measured a few days after a test was a larger crater than had occurred originally. John proposed a geological exploration of the PPG test sites to determine whether his

John G. Lewis

postulate was correct. As a result of a 2-year exploration led by the U.S. Geodetic Survey, John's premise was proven correct. By then, silo basing had won out anyway for other reasons, but John's contribution had enormous impact for the science.

John had a strong influence on me, to say the least. We became acquainted in the late 1950s when DASA sponsored some research programs with Illinois Institute of Technology Research Institute (IITRI) where I worked. In later years, I participated on some of John's technical advisory groups, particularly during the Safeguard anti-ballistic missile program. I left IITRI in 1970 and spent the next 4 years on extended sabbatical in Israel. When John decided to retire from DNA, he asked me if I would be interested in applying for his job, and I followed his suggestion. In 1974, I took over John's position as Chief of the Strategic Structures Division at DNA, and John moved on to sunny Los Angeles with RDA. We worked together ever since. I share with his family this great loss.

by Henry F. Cooper

In late October 1964, I reported for duty at the Air Force Weapons Laboratory on Kirtland Air Force Base in New Mexico, a key turning point in my life. I'll never forget my introduction, shortly after my arrival and before I had time to meet most of my AFWL colleagues and to clutter my desk with papers and punch cards, to the DASA long-range planning process led by John Lewis.

The entire community was assembled in an auditorium to review how each investigator was spending "John's" money—it reminded me of my PhD oral exam, with penetrating questions and (sometimes caustically critical) comments by any and all—monitored at the front table by John and his close advisors who were national leaders in the field of nuclear weapons effects research and testing: Nate Newmark, Fred Sauer and Hal Brode in particular. And everyone entered the fray to challenge and critique everyone else, regardless of rank, seniority or station.

It was extraordinary. And it helped foster a spirit among us "young bucks" to accomplish extraordinary things in rapid order in ways that can be only imagined today. And John subsequently lavished his trust in me and my efforts, including in supporting him on several of his underground nuclear tests and in setting the criteria for the Safeguard system for the Army.

When my tour was up, John invited me to work directly for him at DASA (or maybe it was the DNA by then). But I was in the midst of a major Air Force effort to assess the survivability Air Force's Minuteman system and felt it would be better addressed from a Scientific Advisor post at the AFWL.

It wasn't long until I found myself at odds with the Minuteman System Project Office (SPO) over a particular issue. Ultimately I went to senior DOD officials, including folks I had met because of John's support in earlier issues, and John assembled outside experts to review my concerns. Happily they sided with me, and the Air Force fixed the problem.

Instead we turned to major programs to assure these concerns were taken into account in the billion dollar Minuteman Upgrade Program and in initiating a simulation development program to help design and test a more survivable replacement for the Minuteman system. Again, John was a critical supporter of this important effort which eventually morphed into a key part of the Reagan Strategic Modernization Program in the 1980s.

During the 1970s, we finally worked together at Research and Development Associates (RDA), until I reentered government service. Regrettably, we saw far too little of each other after then.

In reflecting on these memories and others too numerous to review in any detail, I am reminded of the extraordinary qualities of this man who mentored me in my early years. While he was never loud or demanding, he was persistent and fearless in pursuing the things he cared about. He found ways to work with and through (and even around) people, a skill not shared by many I have met. He was an embodiment of the saying attributed to Ronald Reagan—"There is no limit to the amount of good you can do if you don't care who gets the credit."

I was privileged to call him friend—and I regret that I did not tell him that one more time in person.

Lifetime of Trapped Relativistic Electrons in HANE-Generated Radiation Belts

by G. Ganguli, C. Crabtree, M. Mithaiwala (Naval Research Laboratory), and L. Rudakov (Icarus Research Inc.)

The lifetime of trapped relativistic electron flux, created as the fission byproduct in a high-altitude nuclear explosion (HANE), determines the lethality of the resulting radiation belts. The cumulative effect of the enhanced radiation dosage during traversal through the nuclear-enhanced radiation belts can disable critical space assets within weeks. Accurate estimate of the energetic electron lifetime is necessary for developing the standard for remediation techniques, such as satellite hardening or reduction of the radiation level by injection of electromagnetic waves (Ganguli, et al., 2007; Inan, et al., 2003). The lifetime of the trapped electrons is dependent on nonlinear (NL) plasma processes that are prevalent in a post-HANE environment. In particular, the NL scattering of very low-frequency (VLF) waves could play a decisive role (Ganguli, et al., 2010; Crabtree, et al., 2012). A thorough understanding of the relevant nonlinear processes is required for accurate radiation belt models. To achieve this it is necessary to invoke the turbulence theory.

Quasilinear theory is the primary tool used to explain the dynamics of electron fluxes in the radiation belts. Quasilinear analysis is also the first step in the more general method of weak turbulence theory where the waves have random phases and the electron distribution function is solved perturbatively to include nonlinear effects. Figure 1 illustrates a few important interactions in weak turbulence theory. Linear/quasi-linear theory is the interaction of many waves with particles and is self-consistent but does not include nonlinear effects due to the larger amplitude of waves. Resonant nonlinear wave–wave interactions, e.g., decay and coalescence, are where many waves interact in triplets and must satisfy energy ($\omega_{k1} + \omega_{k2} = \omega_{k3}$) and momentum ($\vec{k}_1 + \vec{k}_2 = \vec{k}_3$) conservation. NL scattering (also known as nonlinear Landau damping or nonlinear induced scattering) is the interaction of pairs of waves with plasma particles. While energy and momentum conservation in decay and coalescence processes involve only the waves (the plasma is a passive enabling medium), in induced NL scattering the plasma plays an active role by participating in the momentum and energy conservation.

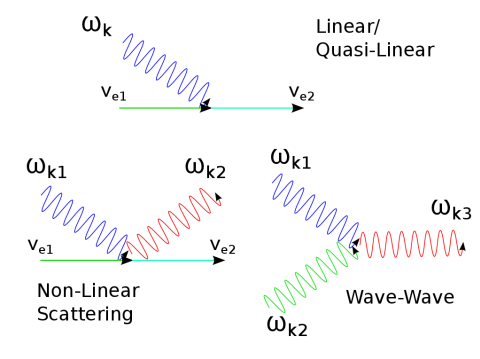

Figure 1. A few different types of interactions in a turbulent plasma.

The nonlinear effects are introduced through a slow density perturbation due to the ponderomotive force when wave amplitude is sufficiently large. For the VLF waves with frequency, ω ($\Omega_i < \omega < \Omega_e$, $\Omega_{i\,e}$ are ion, electron gyrofrequency), this may be calculated using the Vlasov equation in the drift approximation for the electrons, fluid equations for the effectively unmagnetized ions, and the quasineutrality condition (Ganguli, et al., 2010; Mithaiwala, et al., 2011) as,

$$\gamma_{NL} \sim \frac{\Omega_e^2}{n_0 T_e} \frac{\bar{k}^2}{1+\bar{k}^2} \sum_{k1} \frac{(\vec{k}_1 \times \vec{k})_\parallel^2}{k_{1\perp}^2 k_\perp^2} \frac{\bar{k}_1^2}{1+\bar{k}_1^2} \frac{\zeta \,\mathrm{Im}\, Z(\zeta)}{\left(1+(\omega_{k1}-\omega_k)^2/(\vec{k}_1-\vec{k})^2(T_i/M)\right)^2} N_{k1}, \qquad (1)$$

where Z is the plasma dispersion function, $\zeta = (\omega_{k1} - \omega_k)/(k_{1\parallel} - k_\parallel) v_{te}$, M is the ion mass, $\bar{k}^2 = \bar{k}_\perp^2 + \bar{k}_\parallel^2$ is the wave-vector with $(\bar{k}_\parallel, \bar{k}_\perp) = c/\omega_{pe}(k_\parallel, k_\perp)$, ω_{pe} is the plasma frequency, $N_{k1} = W/\omega$ is the plasmon number density, and W is the wave energy density. Equation 1 is the rate of change of the energy contained in waves with $(\bar{k}_\parallel, \bar{k}_\perp)$ due to all other waves with different frequencies, ω_{k1}, and wave-vectors, $\vec{k}_1$, hence the summation. NL scattering can significantly affect wave energy transport and distribution. For example, as long wavelength whistler mode flux propagates in the magnetosphere and approaches the lower-hybrid (LH) resonance surface it becomes increasingly electrostatic with large perpendicular wave-vectors (Edgar, 1976). This increases the NL scattering rate faster (since $\gamma_{NL} \propto k_\perp^4$) than the damping rate (since $\gamma_L \propto k_\perp^2$). Consequently the wave can be scattered before

Lifetime of Trapped Relativistic Electrons in HANE-Generated Radiation Belts *(continued)*

it can be dissipated by linear damping. Upon scattering the wave packet can return toward the Earth and evolve into a long wavelength electromagnetic whistler/magnetosonic wave where it is reflected back towards the magnetosphere, albeit with some loss, and the cycle repeats (Crabtree, et al., 2012). This constitutes the formation of a long-lasting wave cavity in the radiation belts in which whistler waves can be maintained for a long duration thereby increasing the wave-particle interaction time. Thus, NL scattering becomes a major contributor to the radiation belt dynamics by forming a long-lasting cavity in which the VLF waves, which would have dissipated at the lower hybrid surfaces, traverse between the ionosphere and the lower hybrid surface multiple times (Figure 2). Repeated scattering within the cavity maintain the waves at a small average wave-normal angle, which promotes efficient pitch angle scattering and hence shorter life-time for the trapped electrons.

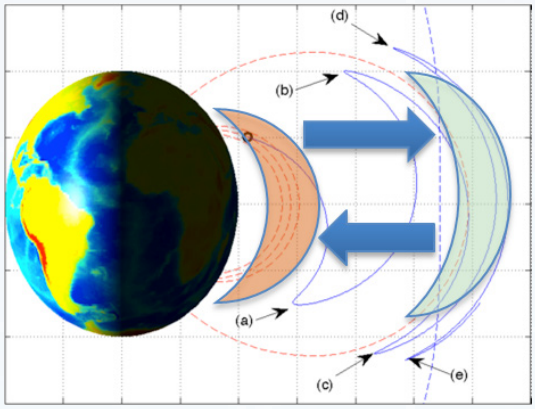

Figure 2 Formation of wave cavity due to NL scattering near LH surface (green region) and reflection from ionosphere (orange region)

Another major effect of the NL scattering is that it enables extraction of the free energy from the post-HANE anisotropic energetic electron distribution through cyclotron resonance. This becomes possible because the wave-particle interaction time is the wave lifetime inside the cavity, which could be orders of magnitude longer than the single pass wave-particle resonance time (Kennel and Petschek, 1966). Consequently, multi-pass gain in the whistler amplitude becomes possible using the free energy from the trapped electron flux (Ganguli, et al., 2012). The extracted energy deposited into the waves enhances the pitch angle scattering rate and can result in prompt electron dropouts.

To illustrate the nonlinear effects consider the kinetic equation for plasmons (Crabtree, et al., 2012; Ganguli, et al., 2012),

$$\frac{\partial N_k}{\partial t}+\vec{\nabla}_{\vec{r}}\left(\frac{d\vec{r}}{dt}N_k\right)+\vec{\nabla}_{\vec{k}}\left(\frac{d\vec{k}}{dt}N_k\right)=\underbrace{Q}_{Source}-2\underbrace{(\gamma_{Coll}+\gamma_L)N_k}_{Linear\ Dampings}+\underbrace{\gamma_{NL}N_k}_{NL\ Scattering}+\underbrace{2\gamma_{LC}N_k}_{Gain}, \qquad (2)$$

where $d\vec{r}/dt=\partial\omega/\partial\vec{k}$ is the plasmon velocity, $d\vec{k}/dt=-\partial\omega/\partial\vec{r}$. Equation 2 follows the trajectory of the wave energy flux through the phase space. The growth rate of the loss-cone instability is,

$$\gamma_{LC}\sim\frac{\pi(\Omega_e/\gamma_R)(n_R/n_e)A}{(1+(k_\perp\rho_e)^3)}, \qquad (3)$$

where $\gamma_R=1/\sqrt{1-v^2/c^2}$ is the relativistic factor, n_e and n_R are the densities of the cold (nonresonant) and energetic (resonant) electrons, ρ_e is the energetic electron gyro-radius, and $A\equiv(T_\perp-T_\parallel)-1$ represents the temperature anisotropy of the trapped energetic electrons where $T_\parallel$ and $T_\perp$ are temperatures parallel and perpendicular to the ambient inhomogeneous magnetic field, $B_0(r)$. A typical ray-path for a whistler wave-packet is shown in Figure 3. The example ray was initiated in the ionosphere at an altitude of 750 km, latitude of 30°, and a frequency of 4 kHz. After 0.7 s, the wave packet is nonlinearly scattered into a new trajectory that returns towards the Earth and the perpendicular wavelength becomes longer. The integrated amplification is due to an unstable loss cone distribution of 1 MeV ($\gamma\sim3$) trapped electrons with $A=1/6$. In the aftermath of HANE the energetic electron flux becomes large, i.e., F(electrons/cm^{2}s) $\sim10^8$ and $n_R\sim10^{-2}$/cc. For ambient $n_e\sim5\cdot10^3$/cc,

Lifetime of Trapped Relativistic Electrons in HANE-Generated Radiation Belts *(continued)*

Figure 4 indicates that most of the amplification occurs within 0.3 s (shaded green in both Figures 3 and 4). After about 0.5 s, the amplification becomes small compared to the damping and the wave-packet begins to lose energy again. The nonlinear scattering occurs at 0.7 s and subsequent amplification is achieved around 2 s. The energy of the wave packet without NL scattering is plotted in blue in Figure 4. We stopped tracking the wave packet before the second NL scattering. Had we continued further, the wave packet would be scattered back towards the ionosphere again and the cycle of amplification process would keep repeating for the duration of the turbulence lifetime. It should be noted that there would be some loss at ionospheric reflections. This illustration demonstrates the potential for extracting a large amount of energy from the trapped electrons for the purpose of rapidly pitch angle scattering them into the loss cone leading to prompt dropouts.

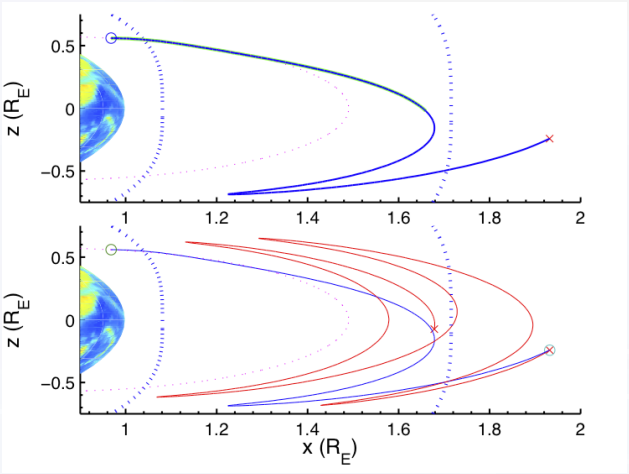

Figure 3. (top) Ray path of wave-packet before NL scattering. Ray path is shaded green for initial portion in which amplification is largest. (bottom) Ray path of wave-packet before NL scattering (blue) and after (red). Oxygen (closer to Earth) and Hydrogen lower-hybrid surfaces are marked with blue dashed lines. Starting L-shell is indicated in magenta dashed line.

The possibility of prompt dropout may partly explain why some detonations led to artificial radiation belts while others did not. In principle, it is possible to access a significant source of free energy introduced by the HANE itself provided seed waves in the right spectrum are present in the aftermath of a HANE. Since the fraction of energy change associated with the wave particle interaction is $\varpi/(\Omega_e/\gamma_R)$ (Kennel and Petschek, 1966), the energy density of the resonant trapped electrons available in a post-HANE environment is $(\varpi\gamma_R/\Omega_e)n_R m\gamma_R c^2 \sim 10^3$ eV/cc. If a small fraction of the available energy is initially extracted by the seed whistlers then an avalanche of energy will ensue. This energy will flow into the turbulence and lead to rapid precipitation of relativistic electrons which will further amplify the waves. This feedback will continue until the trapped resonant electrons are precipitated. Thus, existence (or absence) of seed waves in the right spectrum in the post-HANE environment determines the lethality of the resulting radiation belts.Interestingly, this also holds out the promise of actively reducing the lethality of the nuclear-enhanced radiation belts by injecting electromagnetic waves in the right spectrum with sufficient amplitude in the aftermath of a HANE.

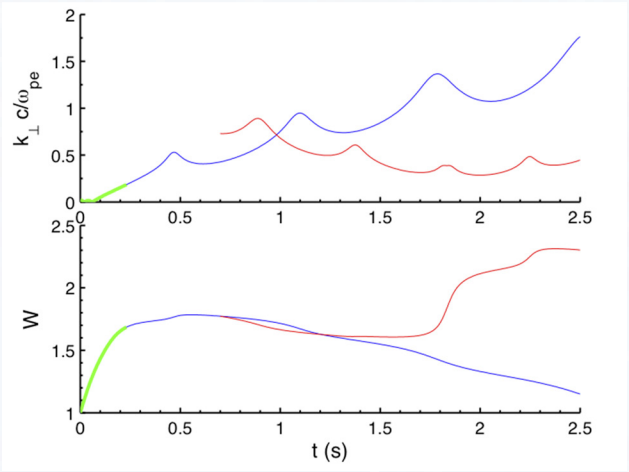

Figure 4 (top) Perpendicular wave-vector without scattering (blue) and with NL scattering (red). (bottom) Energy (in arbitrary units) of wave-packet without scattering (blue) and with NL scattering (red). Green shading for first 0.3 s corresponds to time-period of maximum amplification in the absence of NL scattering.

From the above it is clear that HANE-generated radiation belts are just as dependent on the wave energy distribution and transport as they are on the transport and distribution of the energetic particles. While considerable effort has been directed towards understanding the transport and distribution of energetic particles constituting the radiation belts in the aftermath of a HANE, the corresponding effort for the wave energy flux has lagged. This is due to the difficulty in following the essential microscopic kinetic details of the important nonlinear wave-particle processes globally over the extensive volume of inhomogeneous radiation belts. Particle-in-cell (PIC) simulations can accurately investigate the relevant microscopic kinetic processes (Wintske and Daughton, 2012) but are impractical for global application. Fluid

Lifetime of Trapped Relativistic Electrons in HANE-Generated Radiation Belts *(continued)*

formalisms are better suited for global coverage but they cannot address the important kinetic processes that are critical to the wave energy dynamics. To circumvent these difficulties we are developing wave-in-cell (WIC) simulation model which solves the wave kinetic equation, Equation 2, globally. The advantage of this method is that particle dynamics of the medium is included only through the dispersion relation and hence it is not necessary to resolve the plasma frequency and Debye length. The cell size is governed by the wavelength of the waves and hence can be much larger in size. The time step can be long since the growth/decay/scatter rates are small compared to plasma frequency, cyclotron frequency, and relevant drift frequencies. Equation 2 is solved in each cell. The output, i.e., an upgraded spectrum of wave energy and the NL scattering rate, is transported to the adjoining cells. The upgraded spectrum can then be used to solve the Fokker-Planck equation for the particle distribution. The particle distribution in turn is used to compute the wave growth/damping/scattering, which are then used in the wave kinetic equation to obtain an upgraded spectrum and so on. This way it is possible to follow the wave spectrum and the resulting particle distribution self-consistently over the entire radiation belt as long as the location and spectrum of waves are specified initially in the source term, Q.

This work is supported by DTRA and NRL Base Funds.

References

Crabtree, C., L. Rudakov, G. Ganguli, M. Mithaiwala, V. Galinsky, and V. Shevchenko, (2012), *Physics of Plasmas,* 19, 032903, http://dx.doi.org/10.1063/1.3692092.

Edgar, B. (1976), *J. Geophys. Res,* 81, 205.

Ganguli, G. L. Rudakov, C. Crabtree, M. Mithaiwala. (2012), *Geophys Res Lett.,* 2012, DOI: 10.1029/2012GL052942

Ganguli, G., L. Rudakov, M. Mithaiwala, and K. Papadopoulos, (2007), *J. Geophys. Res,* 112, A06231, doi:10.1029/2006JA012162.

Ganguli, G., L. Rudakov, W. Scales, J. Wang, M. Mithaiwala, (2010), 17, 052310, doi:10.10631/1.3420245.

Inan, U.S., T. F. Bell, J. Bortnik, and J. M. Albert, (2003), *J. Geophys. Res,* 108(A5),1186, doi:10.1029/2002JA009580.

Kennel, C.F., and H. E. Petschek, (1966), *J. Geophys. Res,* 71, 1.

M. Mithaiwala, L. Rudakov, G. Ganguli, C. Crabtree, (2011), *Physics of Plasmas,* 18, 055710, http://dx.doi.org/10.1063/1.3574389

Rudakov, L. C. Crabtree, M. Mithaiwala, G. Ganguli, (2012), arXiv:1211.6392.

Winske, D. and W. Daughton, (2012), *Physics of Plasmas,* 19, 072109.

Investigating Nuclear-Enhanced Artificial Radiation Belt Dynamics in the Laboratory

by W. E. Amatucci, E. M. Tejero, D. D. Blackwell (Naval Research Laboratory), C. D. Cothran (Sotera Global Defense Solutions), and C. L. Enloe (United States Air Force Academy)

High-altitude nuclear testing has revealed that long-lived artificial radiation belts generated in the aftermath of a detonation present a serious threat for disabling low Earth-orbiting (LEO) satellites. The enhanced belts are formed when high energy particles become trapped on stable orbits within the Earth's magnetic field and can persist for years. The particle levels can exceed those of Earth's natural radiation belts by several orders of magnitude. The threat to LEO satellites results from their exposure to greatly increased radiation levels and the rapid accumulation of lethal doses in critical spacecraft components.

In Earth's natural radiation belts, energetic particle levels are controlled by interactions with the electromagnetic fields associated with waves that travel through the ionized gases that comprise the magnetospheric plasma environment. Plasma waves can scatter electrons away from their stable orbits onto paths that lead to the harmless loss of the detrapped particles to the atmosphere. Satellite observations indicate that both whistler waves and electromagnetic ion cyclotron (EMIC) waves are important sources of energetic particle scattering (e.g., Miyoshi, et al., 2008; Ganguli, et al., 2010).

Investigating Nuclear-Enhanced Artificial Radiation Belt Dynamics in the Laboratory *(continued)*

The purpose of the laboratory investigation described here is to better understand the detailed physics controlling the interactions of plasma waves interacting with energetic particles. By creating controlled laboratory plasmas, carefully scaled to space conditions, the scattering of energetic particles by EMIC and whistler waves can be investigated with high spatial and temporal resolution. These efforts provide a unique opportunity to benchmark theoretical and computational models being applied to the radiation belts. The main goals of the laboratory experiments are to

- characterize the wave-vector spectra in scaled radiation belt conditions,
- investigate wave-energetic particle interactions and pitch-angle scattering, and
- measure the loss rates of energetic electrons as wave parameters are varied.

The experiments are being performed at the Naval Research Laboratory in the Space Physics Simulation Chamber, a large-scale experimental device dedicated to the investigation of near-Earth space plasma phenomena (Figure 1). Antennas developed in NRL radiation belt remediation experiments (Amatucci, et al., 2011; Blackwell, et al., 2010; Amatucci, et al., 2005) are used to launch waves with specific frequencies and wavelengths, allowing the key physics associated with electron scattering to be isolated. In other cases, spontaneously generated waves are created by producing plasma equilibria similar to those found in the geospace environment (Tejero, et al., 2011). Control over the physical location of wave generation within the experimental volume has been demonstrated, controlling the spatial location where the wave-particle interactions ultimately will take place.

Within the natural radiation belts, the lifetime of a trapped energetic electron is proportional to the average power density of waves that resonate with the particle. For a wave to scatter a particle, the wave and particle have to stay in phase sufficiently long for the particle trajectory to be appreciably altered. Therefore, the ability to control the wave vector spectrum and the subsequent resonant interaction is critical for any laboratory investigation of electron pitch-angle scattering.

Figure 2 shows a schematic diagram of the experimental setup. A hollow cathode electron source will inject energetic particles with energy variable up to 10 keV. The particles can be injected into the experimental region with controllable angle relative to the background magnetic field (pitch angle). The independent control over energy and pitch angle allow for specific portions of the overall radiation belt particle population to be investigated in detail. Figure 2 also shows a photograph of the electron beam being injected into the Space Chamber and the particles gyrating about the magnetic field. For these experiments, the Space Chamber magnetic field is formed into a half-mirror configuration in order to reflect the

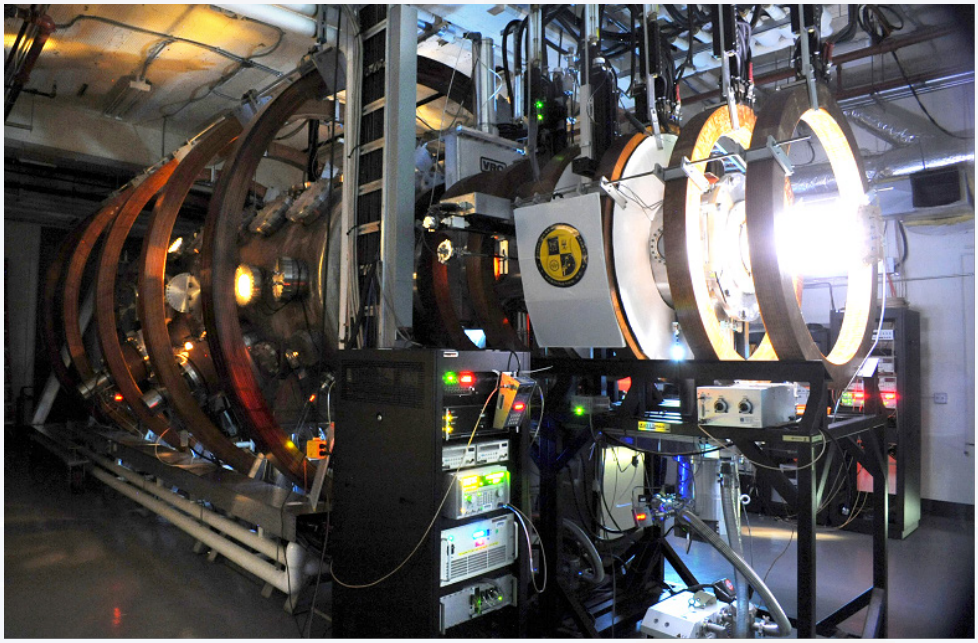

Figure 1. The NRL Space Physics Simulation Chamber in operation. Plasmas scaled to space plasma conditions are produced within this large-scale laboratory device in order to investigate various space plasma phenomena and to develop and test instrumentation for space flight. In these experiments, the interaction of plasma waves with radiation belt particles is investigated.

Investigating Nuclear-Enhanced Artificial Radiation Belt Dynamics in the Laboratory *(continued)*

energetic electrons, simulating the process at one of the poles in the Earth's magnetic field.

By converting from a half to a full magnetic mirror configuration, a situation analogous to particle precipitation in space is created, where energetic electrons will be lost from this trap only if they have a sufficiently large parallel velocity component. Prior to initiating the electron pitch-angle scattering experiments, we first characterize the lifetime of trapped electrons in the mirror configuration as a function of initial pitch angle in both vacuum and quiescent plasma. Lifetime is measured by energetic electron flux detectors placed just beyond the reflection point in the magnetic mirror. Particles can only reach the flux detector when they have been scattered into the loss cone portion of the electron distribution function. Following characterization of trapped electron lifetime in quiescent conditions, pitch-angle scattering by the plasma waves can be investigated. In the experiments, scattering effectively moves the mirror point farther from the magnetic field midplane, analogous to electrons mirroring at lower auroral zone altitudes and being scattered and lost in the neutral atmosphere.

In addition to merely looking for the loss of particle from trapped orbits, detailed measurements of subtle changes in the angle of the scattered electrons after interaction with the waves will be measured by a direction-sensitive electron energy analyzer specifically developed for this purpose. This will enable the migration of the particles from the trapped population into the loss cone of the distribution to be observed. These diffusion rates are a key metric for benchmarking theoretical and computational models of the scattering process. Such laboratory validation provides low-cost risk reduction for future ground and space-based programs to test wave-induced energetic particle precipitation. The laboratory effort will help guide, as well as benefit from, the theoretical and numerical studies, which can then be applied with greater confidence to the in situ environment.

References

Amatucci, W. E., D. D. Blackwell, D. N. Walker, G. Gatling, and G. Ganguli, "Whistler wave resonances in laboratory plasma," IEEE Trans. Plasma Sci., 39, pp. 637-643 (2011).

Amatucci, W. E., D. D. Blackwell, D. N. Walker, G. Gatling, and G. Ganguli, "Whistler wave propagation and whistler wave antenna radiation resistance measurements," IEEE Trans. Plasma Sci., 33, pp. 637-646 (2005).

Blackwell, D., D. Walker, W. Amatucci, "Whistler wave propagation in the antenna near and far fields in the NRL Space Physics Simulation Chamber," *Phys. Plasmas*, 17, Art. No. 012901 (2010).

Ganguli, G, L. Rudakov, W. Scales, J. Wang, and M. Mithaiwala, "Three dimensional character of whistler turbulence," *Phys. Plasmas*, 17, Art. No. 052310 (2010).

Miyoshi, Y., k. Sakaguchi, K. Shiokawa, D. Evans, J. Albert, M. Connors, and V. Jordanova, "Precipitation of radiation belt electrons by EMIC waves, observed from ground and space", *Geophys. Res. Lett.*, 35, L23101 (2008).

Tejero, E., W. Amatucci, G. Ganguli, C. Cothran, C. Crabtree, and E. Thomas, "Spontaneous electromagnetic emission from a strongly localized plasma flow," *Phys. Rev. Lett.*, 106, Art. No. 185001 (2011).

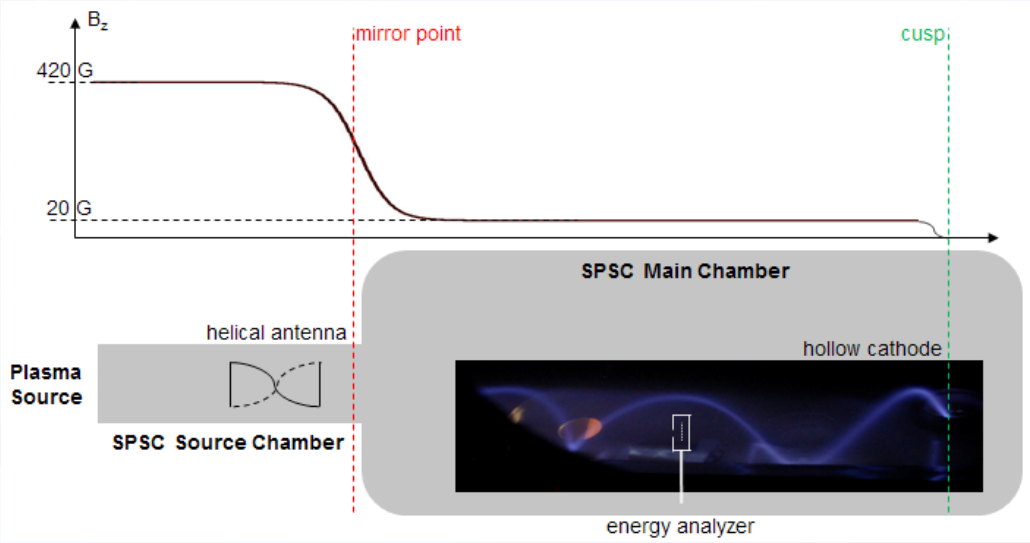

Figure 2. Schematic diagram of the experimental setup for the wave-particle interaction studies. Inset photograph shows the energetic electron beam injected into the NRL Space Chamber to reproduce a selected segment of the scaled radiation belt particle population. Plasma waves launched into these particles scatter or energize the particles, which are detected and characterized using sensitive electron energy analyzers.

Electronics Radiation Response Information Center

Defense Nuclear Agency (predecessor to DTRA) established the Electronics Radiation Response Information Center (ERRIC) as the successor to the US Army's Component Response Information Center (CRIC), formerly operated by Harry Diamond Laboratory, to make data readily available to the nuclear and space effects on electronics hardening and hardness assurance communities. A standalone database once accessible on the world-wide web, ERRIC contained over 11,800 data sets of electronic component responses to nuclear and space radiation.

The database included a master index that enabled a user to locate all piece-part data known to ERRIC. It also provided data entry, maintenance, and report writing capabilities. Individual data sets included the device ID, generic ID, manufacturer, test date, and radiation type (neutron, total dose, dose rate effects, or single event effects). In 1995, the data was approved for open publication, and in 1996, the database was placed on the World Wide Web. Database usage soared to 100,000 requests per year; since the data was unclassified and releasable to the public, the requests came from all over the world.

In addition to maintaining the piece-part database, ERRIC compiled a summary of nuclear radiation effects data on large-scale integrated circuits (Summary of Nuclear Radiation Effects Data on Large-Scale Integrated Circuits—1989 Supplement [DASIAC SR 89 041]). Devices cited included memories, microprocessors, and interface or peripheral devices, giving the responses of the devices to neutrons, ionizing dose, and ionizing dose rate. The report supplements Harry Diamond Laboratories reports HDL-DS-80-1 and HDL-DS-84-1 (available as DTIC documents AD A089112 and AD B083453L, respectively). These reports are limited for release to government personnel and contractors only.

Budget cuts and increased information assurance requirements for government databases caused the ERRIC database website to be shut down. To preserve the data and provide for its continued accessibility, the database was incorporated into Scientific Technical Information Archival Retrieval System (STARS) in 2009.

Sample data from the ERRIC database

Generic ID	Device ID	Manufacturer	Test Date	Radiation Type
02	REF-02	ANALOG DEVICES	2001	TOTAL DOSE
1014	RH1014MW	LTC	2001	TOTAL DOSE
1021-5	RH1021-5	LTC	2001	TOTAL DOSE
117	LM117H	NSC	2001	TOTAL DOSE
117	H117H	LTC	2001	TOTAL DOSE
5116	2N5116	STC	2000	TOTAL DOSE
5154	2N5154	STC	2000	TOTAL DOSE
520	CLC520	NSC	2000	TOTAL DOSE
1055	LT1055	LTC	1999	TOTAL DOSE
1056	RH1056AMW	LTC	1999	TOTAL DOSE
1625	UC1625J	UNITRODE	1998	DOSE RATE
2N3421	2N3421JANS	PPC	1998	TOTAL DOSE
2N6802	2N6802	IRC	1998	SINGLE EVENT
139 1	LM139	NSC	1997	NEUTRON

DTRIAC Collection Additions

DTRA-TR-13-50 The Search for New High-Energy-Density Materials
The objectives of this DTRA project were to design, by using first-principles density functional theory, new superhalogens capable of involving inner core electrons in chemical bonding, validate the theoretical predictions by carrying out photoelectron spectroscopy experiments, and use thus validated theory to guide experiments in focused discovery of new high-energy density materials. Superhalogens belong to a class of highly electronegative species composed of a metal atom at the core surrounded by halogen or oxygen atoms and have electron affinities that are substantially larger than those of the halogen atoms.

DTRA-TR-14-4 Effect of Rock Joints on Failure of Tunnels Subject to Blast Loading
This project provided the basis for numerical simulations of tunnel failure under blast loads. The challenges included handling large deformations, complex failure modes, multiple failure planes, and rock joints with various orientations. Meeting these challenges depended critically on developing appropriate constitutive equations for rock, and a robust, efficient numerical procedure for studying failure induced by waves in the host rock interacting with a tunnel. This research formulated constitutive equations that combined continuum and discontinuum aspects of material response in order to capture essential physical features of rock, such as joints and faults with variable strength and orientation, multiple failure orientations, and a spectrum of failure modes that includes axial splitting and various combinations of shear and opening modes. The numerical approach was based on the material-point method (MPM) that handles large continuum deformations, A constitutive model that predicts fractures was combined with MPM to study rock failure in the vicinity of a tunnel. Moreover, a one-dimensional study of the effect of joints on a propagating wave pulse was performed showing the net transmission through a joint set.

DTRA-TR-14-7 Photonic-Networks-on-Chip for High Performance Radiation Survivable Multi-Core Processor Systems
The University of New Mexico has undertaken a study to determine the effects of radiation on Quantum Dot Photonic Integrated Circuits (QDPICs). Over the course of the last year, the constituent IIIN active semiconductor materials and Si-photonic components forming these QDPICs have been designed, grown and fabricated. Photoluminescence studies before and after radiation exposure have been conducted on bare wafer samples for the III-V quantum-confined laser materials to isolate the damage to the active semiconductor materials themselves. Further techniques to probe radiation damage at the wafer level have been highlighted as well as methods to assess performance degradation at the device level. These studies should pave the way towards the quantitative assessment of the survivability of next-generation multi-cell processors based on optical interconnects.

Other Additions to the Collection

DTRA-TR-14-5 iFind Stand-Off Radiation Detection System and voxel1SPEC Micro-Miniature Electronics (This technical report is Distribution B.)

DTRA-TR-14-10 Dynamic Radiation Imaging and Demonstration (DRIAD) (This technical report is Distribution B.)

DTRA-TR-14-13 Performance of Constellation's CT -8000 Human Portable Radiation Detection System (This technical report is Distribution C.)

DTRA-TR-14-17 Improved Combined NBC Detector (This technical report is Distribution C.)

SBIR Phase III Real-time Portable Neutron Spectroscope (NSPECT) (This small-business innovation research is Distribution D.)

DTRIAC Collection Additions *(continued)*

DTRA DD-12-015 HUMMING ROADRUNNER DTRA DD-12-015 (This data disc is Distribution F.)

DTRA DD-13-004 MIDWAY YELLOW 5 DTRA DD-13-004 (This data disc is Distribution D.)

DTRA DD-13-008 DISTINCT COBRA 14 DTRA DD-13-008 (This data disc is Distribution C.)

DTRA TEP 13 003 DISTINCT IGUANA 7 (This test execution plan is Distribution C.)

This Quarter in History

January 1, 1947	The Atomic Energy Commission takes charge of the nation's atomic program.
January 13, 2003	North Korea announces its withdrawal from the Nuclear Nonproliferation Treaty and begins to reactivate its nuclear facilities.
February 13, 1960	France conducts its first nuclear test in the Sahara Desert near Reggane, Algeria.
March 1, 1954	CASTLE BRAVO was detonated at Bikini Atoll. The detonation resulted in a larger yield than expected (the largest yield in U.S. tests). Inhabitants of nearby islands were evacuated due to dangerous levels of nuclear fallout radiation. The test raised concerns of atmospheric testing
March 1, 1962	The first joint United States–United Kingdom nuclear test, Shot NOUGAT-PAMPAS, was performed at NTS.

Ask the IAC

What is the Process to Publish a Technical Report?

It is DTRA policy to establish and maintain a coordinated and comprehensive scientific and technical information (STI) program that documents the results and outcomes of research and engineering efforts and provides access to those efforts in an effective manner consistent with the DOD mission. Preparing, presenting, and preserving technical reports is a significant part of accomplishing this goal.

To ready a technical report for submission to DTRIAC, the program manager completes a DTRA Form 58, *Scientific & Technical Review Information*, and submits the form and the report for a secuirty review. After the security review is complete, the report is submitted to the DTRIAC STI Support Center (STISC), where it is assigned a report number. This number is significant for universal library and tracking purposes. Next, the report is edited and formatted in accordance with ANSI/NISO Z39.18-2005, Scientific and Technical Reports—Preparation, Presentation and Preservation, and DTRA standards. Once the report is publication ready, STISC submits the report to DTRA Reprographics if hard copies are needed and sends an electronic copy with supporting files to DTRIAC ABQ to be uploaded into the STARS database for secondary distribution purposes. Concurrently, a copy of the report is sent to the Defense Technical Information Information Center (DTIC) as mandated by DOD policy for S&T data.

Questions related to submitting technical reports can be directed to Mr. Ryan Moss in STISC at ryan.moss_contractor@dtra.mil or (703) 767-6684.